Hierarchical relaxation in frustrated systems

N.S. Sullivan[a,*], M. Pilla[b], E.B. Genio[c], J.A. Hamida[a], and K.A. Muttalib[a]
[a]Department of Physics, University of Florida, Gainesville, FL, United States
[b]Qorvo Inc., Richardson, TX, United States
[c]KETD East Qianjin Road Enterprise Science & Technology Park, Kunshan, China
*Corresponding author: e-mail address: sullivan@phys.ufl.edu

Contents

1. Introduction 1
2. The frustrated molecular glass 2
3. Hierarchical dynamics: Quantum rotor glass 10
4. Classical quadrupolar glasses 13
5. Frustrated Bose glass dynamics 15
6. Conclusion 20
Acknowledgments 20
References 20

Abstract

We present a review of the role of hierarchical relaxation processes on the dynamics of geometrically frustrated systems and specifically the low temperature dynamics of the glass states of solid ortho-para hydrogen, orientational and quadrupolar glasses, and solid N_2–Ar mixtures. Comparison is made with the dynamics observed for the recently discovered Bose glass states.

1. Introduction

This contributed article is dedicated to *John R. Sabin* whose wisdom and sound common sense have been very influential on many occasions. Several years ago, researchers were struggling to understand the dynamical behavior observed in the quadrupolar glass state of solid ortho-para hydrogen mixtures for which the local ordering was that of an ensemble of quantum rotors. Jack's advice was to reduce the problem to its simplest terms and then look for the underlying physics. This advice resulted in treating the dynamics as a hierarchical process in which low energy states in a complex

Advances in Quantum Chemistry
ISSN 0065-3276
https://doi.org/10.1016/bs.aiq.2022.07.002

configurational space must be accessed before higher energy states. This approach was able to explain a range of experimental data and was recently invoked to describe the anomalous frequency dependence of the dynamics of a frustrated Bose glass. In this review, we will sketch the progress in understanding the basic features of the relaxational dynamics of three frustrated molecular systems: the quantum rotor glass, the classical orientational glasses, and the simple Bose glass state.

2. The frustrated molecular glass

Of all the molecular glasses, the quadrupolar glass[1–12] formed at low temperatures by dilute mixtures of ortho- and para-hydrogen[13–18] is the most fascinating as the underlying physics is quantum mechanical. The homonuclear diatomic hydrogen can exist as one of two possible species, ortho and para, determined by symmetry. The molecular wave function is the product of a rotational wave function $\Phi_{orb}(J)$, determined by the angular momentum J, and a nuclear wave function $\chi_{nucl}(I)$, determined by the total nuclear spin I which can be 1 or 0. The full wave function $\Psi = \Phi_{orb}(J)\chi_{nucl}(I)$ must be totally antisymmetric. Consequently, ortho-H_2 must have odd values of J and para-H_2 even values of J, as shown in Table 1.

Because of the small moment of inertia, the rotational energies for a hydrogen molecule, $E_J = BJ(J+1)$ with $B = 85.6$ K[19] have a large separation: $E_{J=1} = 171$ K and $E_{J=2} = 510$ K compared to the ground state $J = 0$. In the solid state, we therefore need only consider $J = 1$ and $J = 0$. The anisotropic interactions that can mix the $J = 1$ and $J = 0$ states (principally electrostatic quadrupole–quadrupole interactions[20,21]) are very weak (typically $\approx$1 K) and J may be considered as a good quantum number. Furthermore, the conversion of the ortho species ($J = 1$) to the para species ($J = 0$) is doubly forbidden because two different symmetries (nuclear and rotational) must be broken simultaneously. The ortho-para conversion rate is therefore very slow ($\approx$1.9% per hour[22,23]) and a solid mixture of ortho-para hydrogen will decay very slowly (over a few days) to the pure para state.

Table 1 Symmetry states of nuclear spin species of H_2.

	ortho-H_2	**para-H_2**
χ_{nucl}	Even, $I = 1$	Odd, $I = 0$
Φ_{orb}	Odd, $J = 1, 3, 5\ldots$	Even, $J = 0, 2, 4\ldots$

Only the ortho species ($J = 1$) has orientational degrees of freedom. In the absence of dipolar interactions the dipole moments J_α are expected to vanish for $\alpha = x, y, z$. The five remaining degrees of freedom are in general determined by the expectation values of the operator T_{lm}, which are the operator equivalents of the spherical harmonics Y_{lm} in the manifold $J = 1$. Five parameters are needed to fully specify all the degrees of freedom and we consider two quadrupolar order parameters

$$\sigma_i = (3J_z^2 - 2)_i \text{ and } \eta_i = (J_x^2 - J_y^2)_i \tag{1}$$

for a molecule at site i, with three principal axes x_i, y_i, z_i for the quadrupole moments.

At high ortho-H_2 concentrations, a first-order phase transition occurs from a rotationally disordered state with $\sigma_i = 0$ and $\eta_i = 0$ to an orientationally ordered state at low temperatures. In this orientationally ordered state, the molecules are arranged in an interpenetrating four-sublattice Pa3 structure for which the molecular alignment in each sublattice is along one of the diagonals of a face-centered cubic lattice. This results in a geometrically frustrated system as expected from an orientational ordering driven by electrostatic quadrupole–quadrupole interactions. (For a review see van de Bund and Ackland.[21])

The ordered state is geometrically frustrated because the geometrical alignment of nearest-neighbor molecules does not minimize the short-ranged quadrupole–quadruple interaction for an isolated pair of molecules. Diluting the ortho concentration weakens the orientational ordering and below a critical concentration of about 55%, long range ordering is lost, and the low temperature state is observed to be that of a broad distribution of local order parameters and local axes for the mean alignment at each site as illustrated in Fig. 1.

Some insight into the nature of this order–disorder transition can be obtained from simple molecular field theory.[18] If we assume axial symmetry and a given *mean* local order parameter

$$\sigma = \frac{1}{N}\sum_i \langle 3J_{zi}^2 - 2\rangle \tag{2}$$

we need to evaluate the free energy

$$F(\sigma) = E(\sigma) - TS(\sigma) \tag{3}$$

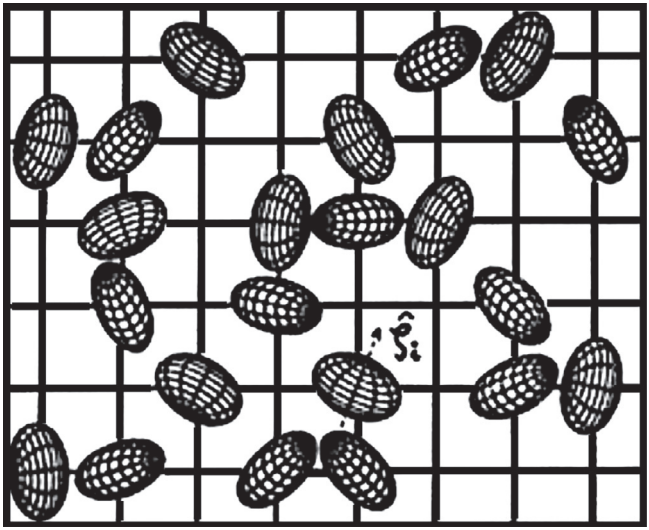

Fig. 1 Schematic representation of a quadrupolar glass as a distribution of prolate and oblate ellipsoids with random directions of principal axes. *After Fig. 4 of Sullivan, N. S.; Devoret, M.; Cowan, B. P.; Urbina, C. Evidence for Quadrupolar Glass Phases in Solid Hydrogen at Reduced Ortho Concentrations. Phys. Rev. B* ***1978****, 17 (12), 5016–5024, https://doi.org/10.1103/PhysRevB.17.5016.*

where S(σ) is the entropy for fixed σ. We then minimize $F(\sigma)$ with respect to σ to find the temperature dependence of σ.

The single particle density matrix can be written as

$$\rho = \frac{1}{3} I_3 + \sum_m T^{\dagger}_{2m} \langle T_{2m} \rangle \tag{4}$$

where I_3 is the unit 3×3 matrix and T_{2m} are the quadrupole operators. (The dipole terms vanish.) With the assumption of axial symmetry, ρ reduces to

$$\rho = \frac{1}{3} I_3 + T_{20} \langle T_{20} \rangle. \tag{5}$$

In the manifold $J = 1$, the ortho-normalized tensor operator is given by

$$T_{20} = \frac{1}{\sqrt{6}} (3J_z^2 - 2). \tag{6}$$

The density matrix becomes

$$\rho = \begin{bmatrix} \frac{1}{3} + \frac{\sigma}{6} & 0 & 0 \\ 0 & \frac{1}{3} - \frac{\sigma}{3} & 0 \\ 0 & 0 & \frac{1}{3} + \frac{\sigma}{6} \end{bmatrix}$$

where the rows and columns are for $J_z = 1, 0, -1$.
The entropy is given by

$$S(\sigma) = Tr(\rho \ln \rho) \tag{7}$$

which becomes

$$\begin{aligned} S(\sigma)) = \frac{1}{3}[&(2+\sigma)\ \ln(2+\sigma) + (1-\sigma)\ \ln(1-\sigma) \\ &- (2+\sigma)\ \ln 2 - 3\ \ln 3]. \end{aligned} \tag{8}$$

The intermolecular quadrupolar interaction between two molecules at sites i and j can be written as

$$\mathscr{H}_{ij}^{QQ} = \sum_{m,n} \Gamma_{ij}^{mn} T_i^{2m} T_j^{2n} \tag{9}$$

where the T^{2m} are the tensorial operators introduced previously and $\Gamma_{ij}^{m,n}$ are interaction constants that depend on the orientations of the local symmetry axes, which are well known for the Pa3 structure.

The quadrupolar interaction varies with molecule separation as r_{ij}^{-5} so we need only consider the mean energy for nearest neighbors. This energy is found to be

$$\langle \mathscr{H}_Q \rangle = 6X\gamma\sigma^2 \tag{10}$$

where γ measures the interaction strength and X is the ortho-H_2 fraction. The total free energy per particle is

$$F(\sigma) = \frac{1}{3} k_B T[(2+\sigma)\ln(2+\sigma) + (1-\sigma)\ln(1-\sigma) - \sigma \ln 2] + 6X\gamma\sigma^2. \tag{11}$$

$F(\sigma)$ is minimized for values of σ that satisfy

$$\frac{36X|\gamma|\sigma}{k_B T} = \ln \frac{(2+\sigma)}{(2-2\sigma)}. \tag{12}$$

For low temperatures the solution is $\sigma_0 = -2$, and as T increases, σ increases toward the value of -1 and then has a discontinuous jump to $\sigma = 0$ at a critical temperature

$$T_C = \frac{18|\gamma|X}{k_B \ln 2}. \tag{13}$$

While this mean-field approach demonstrates the first-order nature of the transition, it is only in qualitative agreement with the observed phase diagram (Fig. 2). It does not explain the origin of the critical concentration below which the glass state appears and the numerical values of T_c are too high.

The first attempt to provide an understanding of the physics responsible for the critical concentration was provided by Kirkwood's method[24,25] of restricted traces carried out to second order. Kirkwood's method is important for the case of quantum rotors because it includes the contributions of correlation terms of the form

$$\langle T_{2m} T_{2n} \rangle. \tag{14}$$

To first order, Kirkwood's method reproduces the mean field result. The second cumulant of Kirkwood's treatment limited to the isotropic terms m, $n = 0$ yields

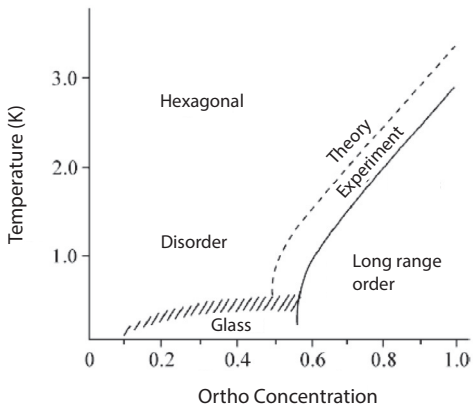

Fig. 2 Phase diagram observed for solid-ortho-para hydrogen mixtures. The hatched region indicates a smooth growth of orientational order into the quadrupolar glass state. *After Fig. 5 from Sullivan, N. S.; Hamida, J. A.; Pilla, S.; Muttalib, K. A.; Genio, E. Molecular Glasses: NMR and Dielectric Susceptibility Measurements. J. Struct. Chem.* ***2016****, 57 (2), 301–307, https://doi.org/10.1134/S0022476616020098.*

$$\begin{aligned} M_2 &= \left\langle \mathscr{H}^2_{QQ} \right\rangle - \langle \mathscr{H}_{QQ} \rangle^2 \\ &= 6N\, X^2\gamma^2(2-\sigma-\sigma^2)[2-\sigma-(2X-1)\sigma^2]. \end{aligned} \tag{15}$$

From this expression, we see that the correlation term changes sign for $X < 0.5$. Detailed calculations that include the anisotropic terms[25] put the critical concentration closer to 55%.

One can use a simple model of a broad distribution of interaction strengths to describe the quadrupolar glass state.[18] Consider the truncated version of Eq. (9)

$$\mathscr{H}_{ij} = \sum_{ij} \Gamma_{ij} T_{20}(i) T_{20}(j) \tag{16}$$

where there is a Gaussian distribution of possible values for the Γ_{ij} given by[26]

$$P(\Gamma_{ij}) = \left(\frac{1}{2\pi\widetilde{\Gamma}^2}\right)^{1/2} \exp\left[-(\Gamma_{ij}-\Gamma_0)^2/2\widetilde{\Gamma}^2\right]. \tag{17}$$

Γ_0 is the mean value of the interaction and $\widetilde{\Gamma}^2$ is the variance. One can now follow the technique of Edwards and Anderson to calculate the free energy by taking an average over an ensemble of n replicas.

$$F = -k_b T \lim_{n\to 0}\left[\frac{1}{n}(\overline{Z^n}-1)\right]. \tag{18}$$

The quadrupolar order parameter is defined as

$$Q = \overline{\langle (T_{20})_\mu)(T_{20})_\nu \rangle}. \tag{19}$$

μ and ν refer to different replicas and the bar represents a configurational average. The local molecular alignment is $\sigma = \overline{\langle T_{20} \rangle}$.

Minimizing F with respect to Q and S, yields

$$\sigma = \left(\frac{1}{2\pi}\right)^{1/2} \int e^{\frac{1}{2}\gamma^2} F(\xi)\, d\gamma \tag{20}$$

and

$$Q = 2 - \sigma - \left(\frac{1}{2\pi}\right)^{1/2} \int e^{\frac{1}{2}\gamma^2} F'(\xi)\, d\gamma \tag{21}$$

with

$$F(x) = \frac{2e^{x} - 2e^{-2x}}{2e^{x} + e^{-2x}} \tag{22}$$

and

$$\xi = \frac{1}{k_B T}\left[\widetilde{\Gamma}(zQ)^{1/2}\gamma + \Gamma_0 z\sigma\right] \tag{23}$$

where z is the number of nearest neighbors.

If $\widetilde{\Gamma} = 0$, one recovers the mean field results

$$Q = 2 - \sigma \tag{24}$$

and

$$k_b T_c = 36\Gamma_0 / \left[\ln \frac{2+\sigma}{2+2\sigma}\right]. \tag{25}$$

On the other hand, for $\widetilde{\Gamma} \gg \Gamma_0$

$$Q = \frac{5}{2} - \frac{27}{2} e^{B^2} erfc(B) \tag{26}$$

with

$$B = 3\widetilde{\Gamma}(zQ/2)^{1/2}. \tag{27}$$

On expanding the error function, one finds a nontrivial Q for

$$k_b T_g = \frac{5}{27}\sqrt{\left(\frac{5\pi z}{3}\right)}\widetilde{\Gamma} = 0.4 z^{1/2}\widetilde{\Gamma}. \tag{28}$$

On estimating $\widetilde{\Gamma}$ by averaging over the angle dependent constants in the electrostatic quadrupole–quadrupole interaction constant one finds for the estimated glass transition[18]

$$T_g = 0.7x^{1/2} \tag{29}$$

which is quite close to the reported values.

The phase diagram was deduced from NMR studies[15,16,27,28] where the NMR line shapes provide a direct measurement of the local order parameters. This property results from the intramolecular nuclear dipole–dipole interaction which in the manifold $J = 1$ can be written as

$$\mathscr{H}_{DD} = hD(3I_Z^2 - 2)\sigma_i(3\cos^2\theta_i - 1) \tag{30}$$

where D is a constant, σ_i is the molecular order parameter, and (θ_i, ϕ_i) define the polar angles for the orientation of the applied magnetic field with respect

to the local symmetry axes. (For simplicity we assume axial symmetry with $\eta_i = 0$ for all i.) Each molecule contributes a doublet to the NMR spectrum at frequencies

$$\Delta f_i = \pm 3D\sigma_i(3\cos^2\theta_i - 1). \tag{31}$$

For a fixed value of σ_i one can sum over the polar angles for a powder sample and one obtains the familiar Pake doublet line shape with two pronounced peaks separated by $6D\sigma_i$. The NMR results were very clear in showing that *both* the local order parameters σ_i and the local axes vary widely in the glass state as represented schematically in Fig. 1. At low temperatures ($T < 0.2$ K) and low ortho concentrations ($X < 0.4$), the observed NMR line shapes correspond approximately to a linear probability distribution of order parameters

$$P(\sigma) \propto \sigma. \tag{32}$$

This linear dependence at small σ is expected since the expression for the entropy is quadratic in σ for small values (Fig. 3).

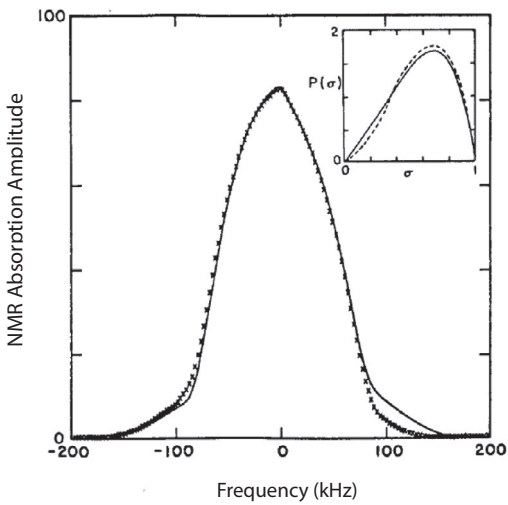

Fig. 3 Fit to the observed NMR line shape at very low temperatures ($T = 44$ mK) for a distribution $P(\sigma)$ of local order parameters σ. There is a small but distinct asymmetry to the line shape and this is due to the nonnegligible nuclear spin polarization (≈6%) at these temperatures. *After Fig. 8 from Edwards, C. M.; Zhou, D.; Lin, Y.; Sullivan, N. S. Local Ordering in Dilute Ortho-Para-Hydrogen Mixtures at Low Temperatures. J. Low Temp. Phys.* ***1988****, 72 (1/2), 1–24, https://doi.org/10.1007/BF00681725.*

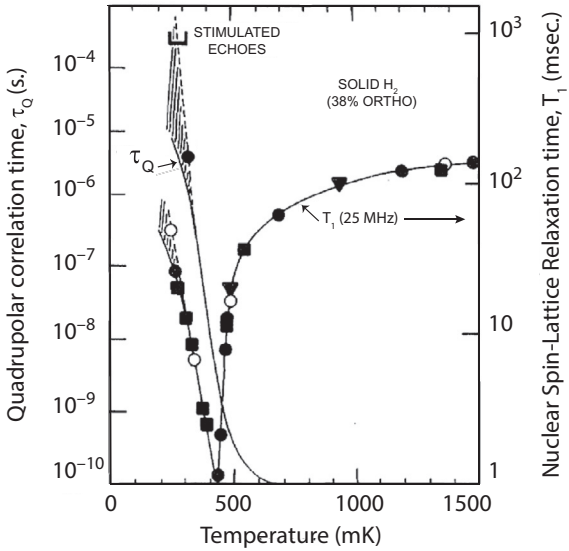

Fig. 4 Rapid variation of molecular relaxation dynamics in quadrupolar glass state of ortho-para hydrogen mixtures, near the transition to the glass state. *After Fig. 1 from Sullivan, N. S.; Estéve, D. Critical Slowing-Down in Spin Glasses: Quadrupolar Glass Phase of Solid H_2. Physica B+C* ***1981****, 107 (1), 189–190, https://doi.org/10.1016/0378-4363(81)90400-9.*

The hashed area in Fig. 2 designates a smooth evolution of the local order parameters from the disordered state to the glass state. There is no sharp discontinuity such as the cusp seen in dipolar spin glasses. There is, however, a very rapid change in the molecular dynamics in the neighborhood of the local glass ordering as shown in Fig. 4.[27,29] This behavior shows that the glass freezing is undoubtedly collective in nature and not simply a para-orientational freezing in fixed local crystal fields.

3. Hierarchical dynamics: Quantum rotor glass

With the continuous evolution of the local order parameters as samples of solid ortho-para hydrogen are cooled into the glass state, the challenge has been to understand the origin of the rapid change in dynamics over a relatively small temperature change. This challenge was addressed by Lin et al.[30,31] who invoked the behavior of the system in the presence of a complex configurational space with a very large number of energy states.

The most striking observation was how the decay of NMR stimulated echoes behaved in the glass state.[32] The decay of these echoes are determined by the spectral density of slow rotational motions (as opposed to the NMR spin-lattice relaxation times which depend on the fluctuations at the nuclear Larmor frequency).

The observed logarithmic decay (see Fig. 5) follows directly from the scaling model of Fisher and Huse.[33,34] The long-time correlations are dominated by the low energy excitations of coherently re-oriented molecules in clusters (or droplets). If E_B is the free energy barrier of a cluster, the tunneling rate to overcome a given barrier at temperature T is

$$W(E_B) = W_0 \exp\left(-\frac{E_B}{k_B T}\right) \tag{33}$$

where W_0 is the characteristic attempt frequency for a given cluster. In the limit of long times (which is the experimental case), W_0 is well defined because it depends on the cluster size. In hierarchical relaxation, the low energy barriers must be crossed first, before the larger barriers can be accessed. In a time t, the energy barriers overcome will therefore be limited to the range

$$0 < E_B < E_{max}(t) \quad \text{where} \quad E_{max}(t) = k_B T \ln(W_0 t). \tag{34}$$

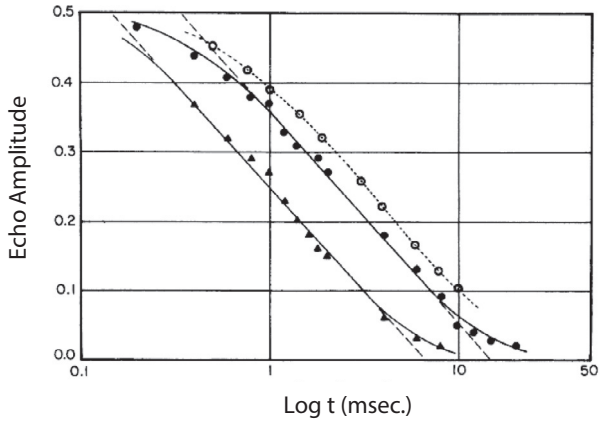

Fig. 5 Logarithmic decay of stimulated echoes in the glass state. The different symbols refer to different pulse periods τ and different samples (*solid circles*: $\tau = 1.7D^{-1}$; *triangles*: $\tau = 3.5D^{-1}$, $X = 0.54$, $T = 0.22$ K; *open circles*: $\tau = 7.7D^{-1}$, $X = 0.43$, $T = 0.15$ K.). *After Fig. 1 from Lin, Y.; Sullivan, N. S. Low-Frequency Dynamics of Orientational Glasses. Phys. Rev. B* ***1988****, 38 (7), 5158–5161, https://doi.org/10.1103/Phys-RevB.38.5158.*

When the barriers are crossed, the local order parameters change significantly and those clusters will therefore not contribute to the NMR stimulated echoes. As a result, the motion associated with barrier crossing erases the orientational *memory* of those clusters. In this scenario, the amplitude of the stimulated echo will therefore be given by

$$A(t) = C\left[1 - \int_0^{E_{max}(t)} \rho(E_B)dE_B\right] \tag{35}$$

where C is a constant dependent on the NMR parameters only, and $\rho(E_B)$ is density of states for rotational energy barriers. At low temperatures, only states with $E_B \approx 0$ need be considered and we have

$$A(t) = C\left[1 - k_B T\rho(0)\ln\left(\frac{t}{t_0}\right)\right] \tag{36}$$

where $t_0 = W_0^{-1}$.

This calculated logarithmic time dependence is not only in good agreement with the NMR results, but it also allows the comparison of the values deduced for the density of states $\rho(0)$ with those deduced from measurements of the heat capacities at low temperatures. For the local quantum rotors $J = 1$, the $J_z = \pm 1$ states are separated from the state $J_z = 0$ by a gap E_B. The broad distribution of low energy states $\rho(E_B)$ therefore leads to a heat capacity given by[14]

$$\frac{C_v}{NR} = \frac{2}{3}k_b TX\int_0^{\frac{3\Delta_0}{k_B T}} \frac{u^2 du}{\left(2e^{-u/2} + e^{u/2}\right)^2}\rho(E) \tag{37}$$

where $u = \frac{3E}{k_B T}$. Fig. 6 shows an excellent agreement of the experimental measurements with the calculated values. At the lowest energies, the density of States $\rho(0) \approx 0.55$ which leads to a predicted stimulated echo decay of

$$A(T)^{calc} = const - 0.28\log_{10}\left(\frac{t}{t_0}\right) \tag{38}$$

which is in good quantitative agreement with the observed decay

$$A(T)^{obs} = const - 0.30\log_{10}\left(\frac{t}{t_0}\right) \tag{39}$$

for a sample with $X = 0.54$ at $T = 0.22$ K.[30–32]

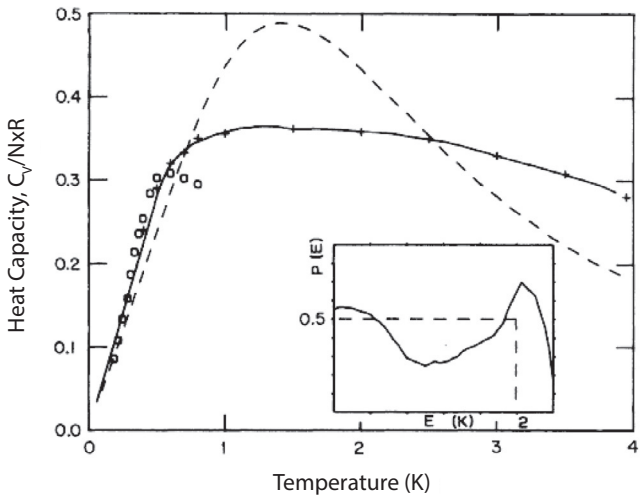

Fig. 6 Comparison of observed and calculated temperature variation of the heat capacity of solid ortho-para H_2 quadrupolar glass state. The symbols refer to experimental data (*crosses*: Engelsberg and Borges,[35] *circles*: Haase et al.[36]). The *broken line* is the prediction for a constant density of states and the *solid line* is the best fit as shown in the inset. *After Fig. 2 from Lin, Y.; Sullivan, N. S. Low-Frequency Dynamics of Orientational Glasses. Phys. Rev. B* ***1988****, 38 (7), 5158–5161, https://doi.org/10.1103/Phys-RevB.38.5158.*

4. Classical quadrupolar glasses

In addition to the quantum rotor glasses formed by solid ortho-para H_2 mixtures at low temperatures, classical rotors in the form of N_2 molecules also transit to orientational glass states at low temperatures when sufficiently diluted with argon.[37–43] A phase diagram very similar to that established for dilute ortho-para H_2 mixtures is observed in solid N_2–Ar mixtures. For high N_2 concentrations ($X > 77\%$), a first-order transition to a Pa3 structure occurs, driven by the quadrupole–quadrupole interactions between N_2 molecules. At lower N_2 concentrations the low temperature state is characterized by a broad distribution of local order parameters (as inferred from NMR line shapes of $^{15}N_2$ molecules) and the crystal lattice structure remains hcp.

At very low N_2 concentrations, $42\% < X < 57\%$, the lattice structure at low temperatures remains fcc and instead of a random distribution of local order parameters, the NMR line shapes are consistent with an approximately fixed value for the local orientational order parameter with the local symmetry axes remaining broadly distributed. The overall phase diagram is shown in Fig. 7.

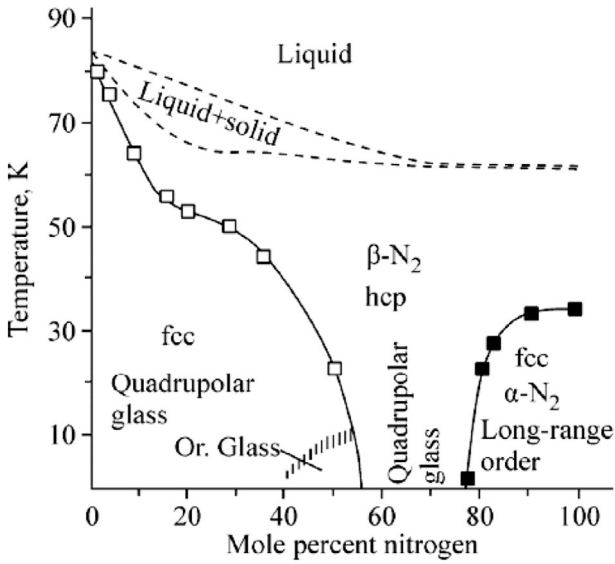

Fig. 7 Phase diagram for solid N_2–Ar mixtures. *After Fig. 4 from Pilla, S.; Hamida, J. A.; Muttalib, K. A.; Sullivan, N. S. Molecular Solid Glasses: New Insights Into Frustrated Systems. New J. Phys.* ***2001****, 3, 17, https://doi.org/10.1088/1367-2630/3/1/317.*

There is special interest in studying the local glass states in sold N_2–Ar mixtures because the order parameters can be probed at very low frequencies using high dielectric measurements of the dielectric susceptibility. This was carried out by Pilla et al.[41,44] using low frequency AC susceptibility measurements. The low frequency dynamics revealed by these measurements exhibit distinct hysteresis loops as shown in Fig. 8. In the long range ordered Pa3 phase, the hysteresis loops are closed and the glass state occurs in a narrow region between $X = 56\%$ and $X = 77\%$. Below $X = 56\%$ the hysteresis loops remain open, indicating that the glass state persists down to the lowest temperatures explored.

In the glass state one can apply a generalized fluctuation-dissipation theorem assuming a model of simple replica symmetry breaking.[45,46] One result of this theorem is that below the glass transition temperature T_G, the area of the hysteresis loop scales as

$$A(\Delta T) \propto \left(\frac{\Delta T}{T_G}\right)^2. \tag{40}$$

Pilla et al.[41,44] showed that the experimental results were in good agreement with this prediction.

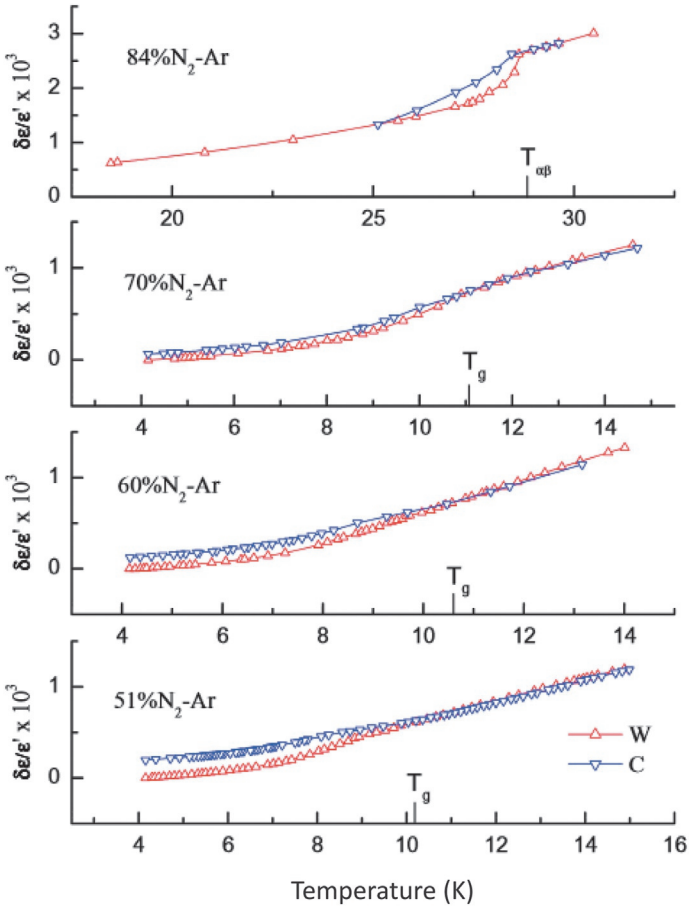

Fig. 8 Evidence for hysteresis in N_2–Ar solid mixtures from measurements of the electric susceptibility ϵ; *W*, warming; *C*, cooling. *After Fig. 1 from Pilla, S.; Hamida, J. A.; Muttalib, K. A.; Sullivan, N. S. Dielectric Response of N_2-Ar Solid Solutions in the Audio Frequency Range. Phys. Rev. B* ***2003****, 67 (17), 174204, https://doi.org/10.1103/PhysRevB.67.174204.*

5. Frustrated Bose glass dynamics

Dichloro-tetrakis thiourea-nickel [$NiCl_2$-$4SC(NH_2)_2$], often referred to as DTN, is a simple quantum molecular magnet exhibiting frustration. It forms a Bose glass state in the presence of disorder which occurs when a small percentage of Cl are replaced with Br.[47,48]

Pure DTN has a body-centered tetragonal crystal structure with the Ni-Cl-Cl-Ni linkage parallel to the c-axis. Thiourea molecules in the ab-plane are linked via hydrogen bonding and are polarizable. The Ni atoms form two interpenetrating tetragonal sub-lattices. Because of high ion anisotropy of the form DS_Z^2, the $S_Z = \pm 1$ states are separated from the $S_Z = 0$ state. Applying a strong magnetic field lowers the energy of the $S_z = +1$ state and when it reaches the energy of the $S_Z = 0$ state an anti-ferromagnetic ordering in the ab-plane occurs.

The magnetic properties of the Ni ions can be described as an ensemble of interacting bosons with $S^- = (2-n)b$, $S^+ = (2-n)b^\dagger$ and $S_Z = n - 1$, with $n = bb^\dagger$. b, $b^\dagger$ are triplet-boson operators and n can be 0,1, or 2. The bosonic interaction Hamiltonian is

$$\begin{aligned}\mathscr{H} = &-\sum_{(ij),c}\sqrt{1-\frac{n_i}{2}}b_i b_j^\dagger\sqrt{1-\frac{n_j}{2}} + h.c.\\ &+\sum_{(ij),ab}\sqrt{1-\frac{n_i}{2}}b_i b_j^\dagger\sqrt{1-\frac{n_j}{2}} + h.c.\\ &+\sum_i D_i(n_i-1)^2 - g\mu_B H\sum_i n_i.\end{aligned} \tag{41}$$

In zero field the large value of D leads to a quantum paramagnetic state, corresponding to a Mott insulator with $n = 1$ particles per Ni atom. The energy gap between the $S_z = 0$ state and the next state is

$$\Delta = D - 2J_c - 4J_{ab}. \tag{42}$$

Applying a magnetic field of strength

$$H_{c1} = \Delta/\mu g \approx 2.1\mathrm{T} \tag{43}$$

closes the gap. Increasing the field beyond H_{c1} leads to an increase in the number of bosons and it is these bosons that condense into a magnetic Bose–Einstein condensate. As the applied field is further increased, the spins cant away from the ab-plane and become saturated at about 12T.

When disorder is added by randomly replacing the Cl linker spins with larger Br spins, a Bose glass[49] is created. The observed phase diagram for 8% Br replacement of the Cl linkers is shown in Fig. 9

In the Bose condensation of the Ni spin excitations in DTN, one observes a strong magneto-electric effect.[50,51] The surprising feature of the Bose glass state is that the observed magneto-electric effect (although

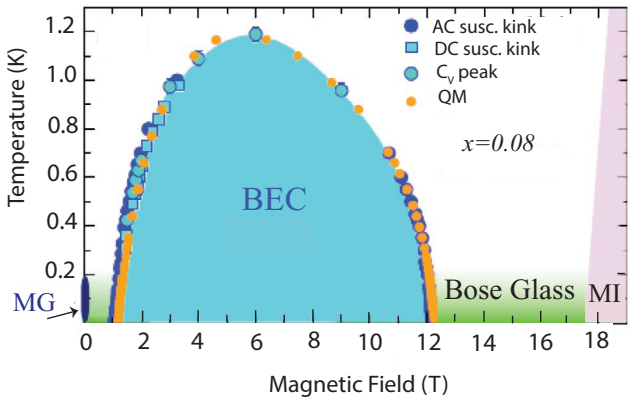

Fig. 9 Phase Diagram for the BEC and Bose glass states for Br (8%) doped DTN. *After Fig. 1 from Yin, L.; Xia, J. -S.; Sullivan, N. S.; Fry, J. N.; Cheng, H. -P.; Yazback, M.; Zapf, V. S.; Paduan-Filho, A. Anomalous Frequency Dependence of Magneto-Electric Effect in Doped DTN. Physica B* ***2021****, 608, 412875, https://doi.org/10.1016/j.physb.2021.412875.*

showing the expected quadratic dependence as a function of applied magnetic field) exhibited a strong peak as a function of frequency near 500 Hz followed by a power law decay as shown in Fig. 10.

As with the case of the frustrated quantum spins ($J = 1$) in the orientational glasses, the frustrated spins in the Bose glass state where there is also disorder, needs to be approached using hierarchical relaxation dynamics. The magnetic susceptibility is measured with an AC electric field applied at frequency f and the change in electric polarization is determined from the impedance change ΔZ in a carefully balanced capacitance bridge.[50] The impedance change at the bridge is

$$\Delta Z = -\frac{1}{2\pi f}\frac{\Delta C}{C_0^2} \tag{44}$$

where ΔC is the change in capacitance due to the sample's dielectric susceptibility and C_0 is the sample cell capacitance. The observed signal from the bridge (reported in Yin et al.[50]) is therefore

$$S = -Kf^{-1}\delta\chi(f) \tag{45}$$

where $\delta\chi(f)$ is the change in susceptibility of the sample for an excitation frequency f, and K is a constant that depends on the sample cell construction.

For hierarchical relaxation, the energy barriers crossed in a time $t = 1/f$ will satisfy

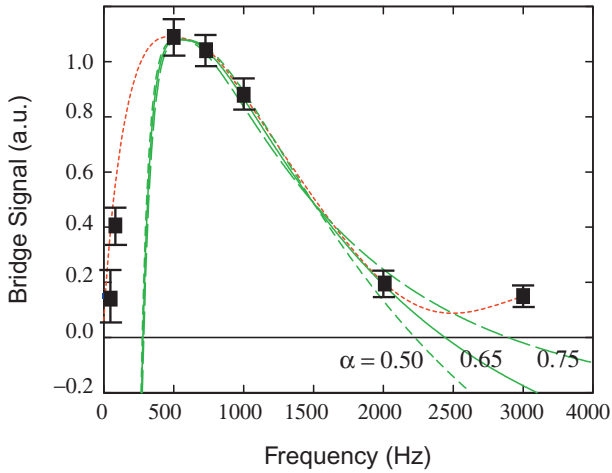

Fig. 10 Anomalous frequency dependence of the magneto-electric effect in the Bose glass state of DTN-Br. The *solid squares* are experimental points. The *dashed*, *solid*, and *broken green lines* are for different power laws with exponent $\alpha = 0.50$, 0.65, and 0.75, respectively. *After Fig. 3 in Yin, L.; Xia, J. -S.; Sullivan, N. S.; Fry, J. N.; Cheng, H. -P.; Yazback, M.; Zapf, V. S.; Paduan-Filho, A. Anomalous Frequency Dependence of Magneto-Electric Effect in Doped DTN. Physica B* ***2021****, 608, 412875, https://doi.org/10.1016/j.physb.2021.412875.*

$$0 < E < E_{max}(t) \tag{46}$$

where

$$E_{max}(t) = k_B T \ln(\Gamma_0 t). \tag{47}$$

Γ_0 is the attempt rate to cross energy barriers and needs to be calculated from the spin–spin interactions in the frustrated state. After the barriers are traversed, the electric polarization beforehand or the memory of the previous states will be erased. The resulting change in electric susceptibility will be

$$\Delta\chi = G\int_0^{E_{max}} \rho(E)dE. \tag{48}$$

Here $\rho(E)$ is the density of spin excitations and G is a constant. Assuming that the density of states is constant at low temperatures (as is the usual case for spin glasses), the frequency dependence of the change in susceptibility is then predicted to be

$$\Delta\chi = k_B T G \ln\left[\frac{\Gamma_0}{f}\right]. \tag{49}$$

The signal recorded by the bridge circuit will then be

$$\Delta Z = -G\frac{k_B T}{f}|\ln\frac{f}{\Gamma_0}|. \tag{50}$$

While this frequency dependence provided a qualitative fit to the experimental data, it does not account for the scaling arguments of Thill and Huse,[52] following the pioneering study of Fisher and Huse.[34] Those scaling arguments showed that the low energy excitations of Ising-like spin glass states that dominate the long-time correlations consist of clusters of "flipped" spins or "droplets" that scale with length as $L^{-\theta}$ where $0 < \theta \leq (d-1)/2$ where d is the effective dimensionality of the excitation system ($d = 2$ for DTN). Fisher and Huse[33,34] considered barrier heights to scale as $B \approx \Delta L^{\Psi}$ and they found that the spin–spin autocorrelation functions scaled as

$$C \approx T\left[\frac{\Delta}{T\ln(t/t_0)}\right]^{\frac{\theta}{\Psi}} \tag{51}$$

where $\theta \leq \Psi \leq 2$. As a result, the frequency-dependence expected for the magneto-electric measurement scales as

$$C(\omega) \approx \frac{k_b T}{\omega}\left|\ln\frac{\omega}{2\pi\Gamma_0}\right|^{\alpha} \tag{52}$$

where the exponent $0 < \alpha < 1$. In Fig. 10, we see that the experimental data is best described by an exponent $\alpha = 0.65$.

The power law behavior with exponent $\alpha < 1$ has also been observed in ordinary spin glasses. Joh et al.[53] showed that the dynamical correlation length for CuMn and $CdCr_{1.7}In_{0.3}S_4$ obeyed the form

$$\xi(t,T) \propto \left[\left(\frac{T}{T_G}\right)\ln(t/t_0)\right]^{1/\Psi} \tag{53}$$

where $1/t_0$ is an attempt frequency to cross energy barriers and T_G is the spin glass temperature. By varying the applied magnetic field, they showed that the states at the barrier height depended on the waiting time t_W with

$$\Delta(t_W, T) = k_B T\ln(t_W/\tau_0). \tag{54}$$

Kisker et al.[54] also reported a similar scaling law for the off-equilibrium dynamics of finite-dimensional spin-glass models.

6. Conclusion

We have considered a wide range of disparate physical systems that have a common feature: the interacting elements (electric or magnetic dipoles, or quadrupoles) are highly frustrated and in the presence of disorder, the landscape of different energy states is a complex array of energy minima and maxima. While some very general and approximate mean field treatments can explain the observed phase diagrams semi-quantitatively, the variation of the dynamics of the system, and in particular the changes as local ordering sets in, can be challenging. In this review we showed how taking Jack Sabin's principle of keeping the underlying driving physics as simple as possible, one can resolve the dynamical behavior and show how it is connected to thermodynamic properties such as the heat capacity. The underlying theme was to invoke hierarchical dynamics as the systems move through configuration space as a function of temperature: low energy barriers must be overcome before attempting to cross high energy barriers. Following this theme, we were able to understand the peculiar logarithmic decay of NMR echoes in the quadrupolar glass state of solid ortho-para hydrogen mixtures and their relation to the heat capacity of those glassy systems. One was also able to understand the behavior of the hysteresis observed for the temperature dependence of the electric susceptibility in solid N_2–Ar mixtures and its relation to replica symmetry breaking in classical orientational or quadrupolar glasses such as solid N_2–Ar mixtures. Finally the anomalous dynamics reported for Bose glass states of the quantum magnet DTN (when diluted with Br) could also be understood in terms of hierarchical relaxation.

Acknowledgments

This work was supported as part of the University of Florida's Center for Molecular Magnetic Quantum Materials, an Energy Frontier Research Center funded by the U.S. Department of Energy, Office of Science, Basic Energy Sciences Program under Award # DE-SC0019330.

References

1 Binder, K. Quadrupolar Glasses. In *Spin Glasses and Random Fields*; Young, A. P., Ed.; World Scientific: Oxford, 1997; pp. 99–108 (Chapter 4).
2 Michel, K. H. Quadrupolar Glasses. *Ferroelectrics* **1988**, *78* (1), 183–189. https://doi.org/10.1080/00150198808215904.
3 Novikov, S. V. Quadrupolar Glass as a Model for Charge Carrier Transport in Nonpolar Organic Materials. *Ann. Phys.* **2009**, *18* (12), 954–958. https://doi.org/10.1002/andp.200910395.

4 Tadic, B.; Pirc, R.; Blinc, R. Local Polarization Distribution in Quadrupolar Glasses. *Phys. Rev. B* **1997**, *55* (2), 816–823. https://doi.org/10.1103/PhysRevB.55.816.

5 Hu, Z.; Garland, C. W.; Wells, A. Elastic Behavior of $K_xNa_{(1-x)}CN$ Quadrupolar Glasses. *Phys. Rev. B* **1989**, *40* (8), 5757–5760. https://doi.org/10.1103/PhysRevB.40.5757.

6 Carmesin, H.-O.; Binder, K. Isotropic Edwards-Anderson Models for Quadrupolar Glasses: A Monte Carlo Simulation. *Europhys. Lett.* **1987**, *4* (3), 269–274. https://doi.org/10.1209/0295-5075/4/3/003.

7 Kokshenev, V. B. Orientational Quadrupolar Glass in Ortho-Para Hydrogen Mixtures. I. Mean-Field Microscopic Theory. *J. Low Temp. Phys.* **1996**, *104*, 1–23. https://doi.org/10.1007/BF00754087.

8 Gribova, N. V.; Tareyeva, E. E. Replica Symmetry Breaking in an Axial Model of Quadrupolar Glass. *Theor. Math. Phys.* **2002**, *131* (3), 852. https://doi.org/10.1023/A:1015983725317.

9 Schelkacheva, T. I. Quadrupolar Glass State in Para-Hydrogen and Ortho-Deuterium Under Pressure. *JETP Lett.* **2002**, *76*, 374–376. https://doi.org/10.1134/1.1525040.

10 Sellar, J. R.; Jeffrey, R.; Chen, C. Y. Metastability, Tetragonality and Quadrupolar Glass States in Cubic Stabilized Zirconia. *J. Am. Ceram. Soc.* **2020**, *103* (10), 5546–5553. https://doi.org/10.1111/jace.17334.

11 Müser, M. H. Computer Simulation of a Quadrupolar Glass. *J. Phys. Condens. Matter* **1996**, *8*, 913–925. https://doi.org/10.1088/0953-8984/8/8/004.

12 Loidl, A. Orientational Glasses. *Annu. Rev. Phys. Chem.* **1989**, *40* (1), 29–60. https://doi.org/10.1146/annurev.pc.40.100189.000333.

13 Mancini, F. P.; Sherrington, D. One-Step Replica Symmetry Breaking Solution of the Quadrupolar Glass Model. *J. Phys. A Math. Gen.* **2006**, *39* (43), 13393–13403. https://doi.org/10.1088/0305-4470/39/43/001.

14 Candela, D.; Buchman, S.; Vetterling, W. T.; Pound, R. V. NMR Lineshapes of the Solid Hydrogen Quadrupolar Glass. *Physica B+C* **1981**, *107* (1), 187–188. https://doi.org/10.1016/0378-4363(81)90399-5.

15 Sullivan, N. S.; Pound, R. V. Nuclear-Spin-Lattice Relaxation of Solid Hydrogen at Low Temperatures. *Phys. Rev. A* **1972**, *6* (3), 1102–1107. https://doi.org/10.1103/PhysRevA.6.1102.

16 Sullivan, N. S.; Devoret, M.; Cowan, B. P.; Urbina, C. Evidence for Quadrupolar Glass Phases in Solid Hydrogen at Reduced Ortho Concentrations. *Phys. Rev. B* **1978**, *17* (12), 5016–5024. https://doi.org/10.1103/PhysRevB.17.5016.

17 Lukierska-Walasek, K.; Walasek, K. Effect of the Zero-Point Rotational Motions on the Quadrupolar Glass Order Parameter in Solid Hydrogen. *Phys. Rev. B* **1994**, *50* (17), 12437–12440. https://doi.org/10.1103/PhysRevB.50.12437.

18 Sullivan, N. S. Orientational Order-Disorder Transitions in Solid Hydrogen. *Can. J. Chem.* **1988**, *66*, 908–914. https://doi.org/10.1139/v88-154.

19 Silvera, I. F. The Solid Molecular Hydrogens in the Condensed Phase: Fundamentals and Static Properties. *Rev. Mod. Phys.* **1980**, *52* (2), 393–452. https://doi.org/10.1103/RevModPhys.52.393.

20 Harris, A. B. Interactions Between Molecules in Solid Hydrogen. *Phys. Rev. B* **1970**, *1* (5), 1881–1902. https://doi.org/10.1103/PhysRevB.1.1881.

21 van de Bund, S.; Ackland, G. J. Quadrupole Arrangements and the Ground State of Solid Hydrogen. *Phys. Rev. B* **2020**, *101* (1), 014103. https://doi.org/10.1103/PhysRevB.101.014103.

22 Ahlers, G. Ortho-Para Conversion Rate in Solid Hydrogen. *J. Chem. Phys.* **1964**, *40*, 3123.

23 Berlinsky, A. J.; Hardy, W. N. Theory of Ortho-Para Conversion and its Effect on the NMR Spectrum of Ordered Solid Ortho-Hydrogen. *Phys. Rev. B* **1973**, *8* (11), 5013–5027. https://doi.org/10.1103/PhysRevB.8.5013.

24 Kirkwood, J. G. Statistical Mechanics of Fluid Mixtures. *J. Chem. Phys.* **1935**, *3* (5), 300–313. https://doi.org/10.1063/1.1749657.

25 Sullivan, N. S. Orientational Ordering in Solid hydrogen. *J. Phys.* **1976**, *37*, 981. https://doi.org/10.1051/jphys:01976003707-8098100.

26 Tareyeva, E. E.; Schelkacheva, T. I.; Chtchelkatchev, N. M. Orientational Glass: Full Replica Symmetry Breaking in Generalized Spin Glass-Like Models Without Reflection Symmetry. *Phys. Lett. A* **2013**, *377* (7), 507–512. https://doi.org/10.1016/j.physleta.2012.12.023.

27 Ishimoto, H.; Nagamine, K.; Kimura, Y.; Kumagai, H. Measurements of Nuclear Spin-Lattice Relaxation Time of Solid Hydrogen in the Ordered State. *J. Phys. Soc. Jpn.* **1974**, *37* (4), 956–960. https://doi.org/10.1143/JPSJ.37.956.

28 Cochran, W. T.; Gaines, J. R.; McCall, R. P.; Sokol, P. E.; Patton, B. R. Study of the Quadrupolar-Glass Region in Solid D_2 Via Proton Magnetic Resonance. *Phys. Rev. Lett.* **1980**, *45* (19), 1576–1580. https://doi.org/10.1103/PhysRevLett.45.1576.

29 Sullivan, N. S.; Estève, D. Critical Slowing-Down in Spin Glasses: Quadrupolar Glass Phase of Solid H_2. *Physica B+C* **1981**, *107* (1), 189–190. https://doi.org/10.1016/0378-4363(81)90400-9.

30 Lin, Y.; Sullivan, N. S. Low-Frequency Dynamics of Orientational Glasses. *Phys. Rev. B* **1988**, *38* (7), 5158–5161. https://doi.org/10.1103/PhysRevB.38.5158.

31 Sullivan, N. S.; Lin, Y. Relaxation and Large-Scale Excitations in the Orientational Glass State of Solid H_2. *Chem. Phys. Lett.* **1989**, *156* (2), 218–222. https://doi.org/10.1016/S0009-2614(89)87123-4.

32 Sullivan, N. S.; Esteve, D.; Devoret, M. NMR Pulse Studies of Molecular Solids: $^{15}N_2$ and H_2. II. Stimulated Echoes and Slow Rotational Motions. *J. Phys. C Solid State Phys.* **1982**, *15* (23), 4895–4911. https://doi.org/10.1088/0022-3719/15/23/024.

33 Fisher, D. S.; Huse, D. A. Nonequilibrium Dynamics of Spin Glasses. *Phys. Rev. B* **1988**, *38* (1), 373–385. https://doi.org/10.1103/PhysRevB.38.373.

34 Fisher, D. S.; Huse, D. A. Ordered Phase of Short-Range Ising Spin-Glasses. *Phys. Rev. Lett.* **1986**, *56* (15), 1601–1604. https://doi.org/10.1103/PhysRevLett.56.1601.

35 Engelsberg, M.; Borges, N. M. Nuclear Spin Stimulated Echoes in Glasses. *J. Phys. C Solid State Phys.* **1984**, *17* (20), 3633–3644. https://doi.org/10.1088/0022-3719/17/20/014.

36 Haase, D. G.; Perrell, L. R.; Saleh, A. M. Specific Heat, Pressure, and the Grüneisen Relation in Solid Hydrogen. *J. Low Temp. Phys.* **1984**, *55* (3), 283–296. https://doi.org/10.1007/BF00683447.

37 Hamida, J. A.; Genio, E. B.; Sullivan, N. S. NMR Studies of the Orientational Ordering in Dilute Solid N_2-Ar Mixtures. *J. Low Temp. Phys.* **1996**, *103* (1), 49–70. https://doi.org/10.1007/BF00754657.

38 Klee, H.; Carmesin, H. O.; Knorr, K. Quadrupolar Glass State of $(Ar)_{1-x}(N_2)_x$. *Phys. Rev. Lett.* **1988**, *61* (16), 1855–1858. https://doi.org/10.1103/PhysRevLett.61.1855.

39 Hamida, J. A.; Pilla, S.; Sullivan, N. S. The Orientational Ordering in Dilute Solid N_2-Ar Mixtures. *J. Low Temp. Phys.* **1998**, *111*, 365–370. https://doi.org/10.1023/A:1022287720183.

40 Manzhelii, V. G.; Bagatskii, M. I.; Minchina, I. Y.; Aleksandrovskii, A. N. Thermodynamic Properties of Molecular Orientational Glasses With Indirect Interaction. *J. Low Temp. Phys.* **1998**, *111* (3), 257–270. https://doi.org/10.1023/A:1022219232478.

41 Pilla, S.; Hamida, J. A.; Muttalib, K. A.; Sullivan, N. S. Molecular Solid Glasses: New Insights Into Frustrated Systems. *New J. Phys.* **2001**, *3*, 17. https://doi.org/10.1088/1367-2630/3/1/317.

42 Suan Li, M.; Gawron, T. R.; Cieplak, M. Scaling Properties of Quadrupolar and Octupolar Glasses. *Phys. Lett. A* **1992**, *164* (1), 120–125. https://doi.org/10.1016/0375-9601(92)90917-B.
43 Müser, M. H.; Löding, D.; Nielaba, P.; Binder, K. Computer Simulations of a Lennard-Jones Model for $Ar_{(1-x)}(N_2)_x$: A Prototype System for Quadrupolar Glasses. *Ferroelectrics* **1998**, *208–209* (1), 293–327. https://doi.org/10.1080/00150199808014882.
44 Pilla, S.; Hamida, J. A.; Muttalib, K. A.; Sullivan, N. S. Dielectric Response of N_2-Ar Solid Solutions in the Audio Frequency Range. *Phys. Rev. B* **2003**, *67* (17), 174204. https://doi.org/10.1103/PhysRevB.67.174204.
45 Cugliandolo, L. F.; Kurchan, J. Analytical Solution of the Off-Equilibrium Dynamics of a Long-Range Spin-Glass Model. *Phys. Rev. Lett.* **1993**, *71* (1), 173–176. https://doi.org/10.1103/PhysRevLett.71.173.
46 Cugliandolo, L. F.; Kurchan, J. Mean-Field Theory of Temperature Cycling Experiments in Spin Glasses. *Phys. Rev. B* **1999**, *60* (2), 922–930. https://doi.org/10.1103/PhysRevB.60.922.
47 Yin, L.; Xia, J. S.; Zapf, V. S.; Sullivan, N. S.; Paduan-Filho, A. Direct Measurement of the Bose-Einstein Condensation Universality Class in $NiCl_2$-$4SC(NH_2)_2$ at Ultralow Temperatures. *Phys. Rev. Lett.* **2008**, *101* (18), 187205. https://doi.org/10.1103/PhysRevLett.101.187205.
48 Pillai, K.; Mun, E.; Wilcox, J.; Manson.; Scott, B.; Tobash, P.; Zapf, V. S. The Origin and Coupling Mechanism of the Magnetoelectric Effect in $TMCl_2$-$4SC(NH_2)_2$ (TM = Ni and Co). *Adv. Condens. Matter Phys.* **2014**, *2014*, 1–4. https://doi.org/10.1155/2014/512621.
49 Yu, R.; Yin, L.; Sullivan, N. S.; Xia, J. S.; Huan, C.; Paduan-Filho, A.; Oliveira, N. F.; Haas, S.; Steppke, A.; Miclea, C. F.; Weickert, F.; Movshovich, R.; Mun, E. D.; Scott, B. L.; Zapf, V. S.; Roscilde, T. Bose Glass and Mott Glass of Quasiparticles in a Doped Quantum Magnet. *Nature* **2012**, *489*, 379–384. https://doi.org/10.1038/nature11406.
50 Yin, L.; Xia, J.-S.; Sullivan, N. S.; Zapf, V. S.; Paduan-Filho, A. Magnetic Susceptibility Measurements at Ultra-Low Temperatures. *J. Low Temp. Phys.* **2010**, *158* (3), 710. https://doi.org/10.1007/s10909-009-0029-2.
51 Xia, J. S.; Yin, L.; Sullivan, N. S.; Zapf, V. S.; Paduan-Filho, A. Magneto-Electric Effect and Dielectric Susceptibility Measurement Technique at Very Low Temperature. *J. Low Temp. Phys.* **2017**, *187* (5), 627–632. https://doi.org/10.1007/s10909-016-1723-5.
52 Thill, M. J.; Huse, D. A. Equilibrium Behaviour of Quantum Ising Spin Glass. *Physica A* **1995**, *214* (3), 321–355. https://doi.org/10.1016/0378-4371(94)00247-Q.
53 Joh, Y. G.; Orbach, R.; Wood, G. G.; Hammann, J.; Vincent, E. Extraction of the Spin Glass Correlation Length. *Phys. Rev. Lett.* **1999**, *82* (2), 438–441. https://doi.org/10.1103/PhysRevLett.82.438.
54 Kisker, J.; Santen, L.; Schreckenberg, M.; Rieger, H. Off-Equilibrium Dynamics in Finite-Dimensional Spin-Glass Models. *Phys. Rev. B* **1996**, *53* (10), 6418–6428. https://doi.org/10.1103/PhysRevB.53.6418.